

# Journal of Materials Chemistry A

Materials for energy and sustainability

Accepted Manuscript

This article can be cited before page numbers have been issued, to do this please use: J. Wang, P. Chong, W. Limphirat, H. Wang, W. Busayaporn, L. Zhang, H. L. Seng, S. Sun, Z. Aabdin, C. Dong, M. Wei and Z. W. Seh, *J. Mater. Chem. A*, 2025, DOI: 10.1039/D5TA03608A.



This is an Accepted Manuscript, which has been through the Royal Society of Chemistry peer review process and has been accepted for publication.

Accepted Manuscripts are published online shortly after acceptance, before technical editing, formatting and proof reading. Using this free service, authors can make their results available to the community, in citable form, before we publish the edited article. We will replace this Accepted Manuscript with the edited and formatted Advance Article as soon as it is available.

You can find more information about Accepted Manuscripts in the [Information for Authors](#).

Please note that technical editing may introduce minor changes to the text and/or graphics, which may alter content. The journal's standard [Terms & Conditions](#) and the [Ethical guidelines](#) still apply. In no event shall the Royal Society of Chemistry be held responsible for any errors or omissions in this Accepted Manuscript or any consequences arising from the use of any information it contains.

## ARTICLE

Received 00th January  
20xx,

Accepted 00th January 20xx

DOI: 10.1039/x0xx00000x

**Hierarchical Vanadium Sulfide Nanosheets with Expanded Interchain Spacings for High Performance Sodium–Ion Batteries**Jianbiao Wang,<sup>\*‡</sup> Peidian Chong,<sup>b‡</sup> Wanwisa Limphirat,<sup>c‡</sup> Haiyi Wang,<sup>a</sup> Wutthikrai Busayaporn,<sup>c</sup> Lei Zhang,<sup>a</sup> Debbie Hwee Leng Seng,<sup>a</sup> Shengnan Sun,<sup>a</sup> Zainul Aabdin,<sup>a</sup> Chaoyu Dong,<sup>d</sup> Mingdeng Wei,<sup>\*b</sup> Zhi Wei Seh <sup>\*a</sup>

Sodium–ion batteries (SIBs) have been intensively researched as potential alternative energy storage devices for lithium–ion batteries (LIBs). Nevertheless, the scarcity of suitable anode materials capable of hosting the large radius of Na<sup>+</sup> has hindered the further application of SIBs. Herein, we developed a hierarchical VS<sub>4</sub> nanosheet with expanded interchain spacing of 0.98 nm without additive for the first time. Additionally, we found that the porous structure in hierarchical VS<sub>4</sub> nanosheet provides sufficient active sites for Na<sup>+</sup> storage and alleviates the volume variation during discharge/charge cycles, as supported by finite element simulations (FES) data. More importantly, a dynamic insertion–dominated storage mechanism was revealed through synchrotron X–ray absorption spectra and X–ray photoelectron spectroscopy. Thus, the optimized anode delivered a high capacity of 441 mAh g<sup>−1</sup> at 1 A g<sup>−1</sup> after 200 cycles. This work provides critical insights into the design of SIBs by correlating storage mechanisms with electrode's structural composition.



Dr. Wang Jianbiao is a Scientist at the Institute of Materials Research and Engineering (IMRE), Agency for Science, Technology and Research (A\*STAR), Singapore. He received his Ph.D. in 2021 from Fuzhou University. From 2019 to 2021, he served as a Special Researcher at Nagasaki University, Japan. His research interests include the development of novel electrode materials, the investigation of energy storage mechanisms involving Li<sup>+</sup>, Na<sup>+</sup>, Mg<sup>2+</sup>, and Zn<sup>2+</sup> ion batteries, and the optimization of electrolyte systems.

<sup>a</sup> Institute of Materials Research and Engineering (IMRE), Agency for Science, Technology and Research (A\*STAR), 2 Fusionopolis Way, Innova #08-03, Singapore 138634, Republic of Singapore.

<sup>b</sup> Fujian Key Laboratory of Electrochemical Energy Storage Materials, Fuzhou University, Fuzhou 350116, China.

<sup>c</sup> Synchrotron Light Research Institute, 111 Moo 6 University Avenue, Muang, Nakhon Ratchasima 30000, Thailand.

<sup>d</sup> Singapore Institute of Manufacturing Technology (SIMTech), Agency for Science, Technology and Research (A\*STAR), 5 Cleantech Loop, 01-01 Cleantech Two Block B, Singapore 636732, Republic of Singapore.

\*Corresponding authors' emails: jianbiao\_wang@imre.a-star.edu.sg; wei-mingdeng@fzu.edu.cn; sehz@imre.a-star.edu.sg.

<sup>†</sup>Supplementary Information available: [details of any supplementary information available should be included here]. See DOI: 10.1039/x0xx00000x

<sup>‡</sup>These authors contributed equally to this work



## ARTICLE

## 1. Introduction

With the massive application of lithium-ion batteries (LIBs), increasing concerns over cost and safety have prompted research interest in alternative energy storage devices, including sodium-ion batteries and multivalent-ion batteries.<sup>1-5</sup> Sodium-ion batteries (SIBs) are considered as a promising alternative, due to their similar redox chemistry to LIBs, as well as natural abundance of sodium.<sup>6-10</sup> Nevertheless, the larger radius of Na<sup>+</sup> than that of Li<sup>+</sup> leads to the sluggish electrochemical kinetics, hampering the practical implementations of SIBs.<sup>11-17</sup>

The electrochemical kinetics of SIBs can be enhanced by employing transition metal sulfides as anodes, owing to their high theoretical capacity and excellent ionic conductivity.<sup>7, 18-20</sup> Among these, VS<sub>4</sub> has been emerged as a promising candidate, as its abundant (S<sub>2</sub>)<sup>2-</sup> anions contribute to high capacity. However, its practical application is hindered by significant volume changes during the discharge/charge process.<sup>21-24</sup> To address this challenge, various strategies have been explored, such as combining VS<sub>4</sub> with MXene or fabricating heterojunction structures.<sup>25</sup> However, achieving high capacity VS<sub>4</sub>-based anodes remains challenging. Ether-based electrolytes with sodium trifluoromethanesulfonate (NaOTF) have been extensively researched in SIBs, due to high reversibility during plating/stripping of Na<sup>+</sup>.<sup>6, 9</sup> A limited understanding of the storage mechanisms of VS<sub>4</sub> in NaOTF-ether electrolytes also further constrain its application in SIBs.

Here for the first time, we synthesized hierarchical VS<sub>4</sub> nanosheets with expanded interchain spacings via a one-step solvothermal process, without the need of any additives. To the best of our knowledge, this work reports the largest interchain spacing for VS<sub>4</sub> to date, offering increased Na<sup>+</sup> storage capacity. Unlike previous studies, we unveiled a dynamic insertion-dominated storage mechanism in the discharge/charge process with NaOTF-ether electrolyte, using synchrotron X-ray absorption spectroscopy (XAS) and X-ray photoelectron spectroscopy (XPS). Additionally, the porous structure provides ample space to accommodate Na<sup>+</sup> and mitigates the volume variation in the insertion/extraction of Na<sup>+</sup>, which enhances structural stability as supported by finite element simulations (FES) data. The presence of nanosheets can effectively reduce the diffusion pathway of Na<sup>+</sup>. Moreover, the composition of solid electrolyte interface (SEI) formed on the surface of VS<sub>4</sub> nanosheets was also investigated using XPS. Thus, a stable electrochemical performance of VS<sub>4</sub> could be achieved. In detail, the hierarchical VS<sub>4</sub> nanosheets anode maintains a high capacity of 441 mAh g<sup>-1</sup> at 1000 mA g<sup>-1</sup> after 200 cycles, showing advantages among VS<sub>4</sub>-based anodes.<sup>19</sup> Based on this work, we found that the interfacial chemistry between electrode and electrolyte is vital for the cycling performance of batteries. Future efforts will focus on investigating and optimizing SEI formation to advance the development of high-energy-density batteries.

## 2. Experimental

### Synthesis of hierarchical nanosheets

For the synthesis of hierarchical VS<sub>4</sub> nanosheets, 1 mmol of NH<sub>4</sub>VO<sub>3</sub> was added into 30 ml of ethanol, stirred for about 5 mins. Then, 4 mmol of thioacetamide was added into the above solution, stirred for another 10 mins. Subsequently, the solution was transferred to 200 °C oven, heated for 12 h. After cooling naturally to room temperature, the black product was collected via centrifugation and washed with ethanol and isopropanol several times. At last, the product was obtained by drying at vacuum oven at 70 °C overnight.

### Electrochemical measurement

Detailed information about electrochemical measurements is found in Supporting Information.

### Material Characterizations

Please see the information of material characterizations in Supporting Information.

### FES simulation method

Finite element simulations were performed using COMSOL software. A hygroscopic model was employed to represent the swelling behaviour resulting from the absorption of Na<sup>+</sup> ions, using a concentration of 1 mol/L. The hygroscopic swelling coefficient was assumed to be 1×10<sup>-3</sup> m<sup>3</sup>/kg. As the parameters may not accurately represent real conditions, the results are intended for



qualitative analysis only. To simulate the displacement distribution caused by swelling, the external surfaces of the nanoparticles were set as free boundaries.

DOI: 10.1039/D5TA03608A

### 3. Results and discussion

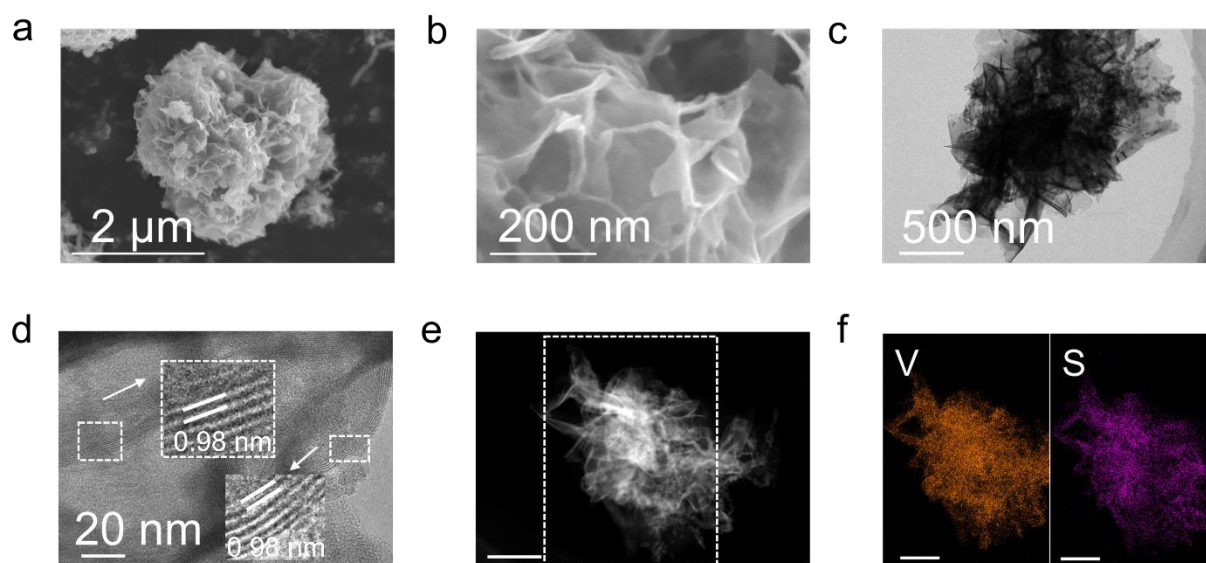


**Fig. 1 Material characterizations:** (a, b) SEM images, (c) TEM image, (d) HRTEM, and (e) STEM image and (f) corresponding elemental maps of V and S in hierarchical  $VS_4$  nanosheets (Scale bar: (e): 500 nm, (f): 500 nm).

Scanning electron microscopy (SEM) and transmission electron microscopy (TEM) images are presented in Fig. 1 to investigate the morphological and structural composition of  $VS_4$ . Hierarchical  $VS_4$  nanosheet with porous structure is observed, where the magnified SEM images reveal the porous structure consists of interconnected nanosheets (Fig. 1a, b). TEM image in Fig. 1c reveals the characteristics of nanosheets. High-resolution TEM (HRTEM) image shows lattice fringes of 0.98 nm, indicating an expanded interchain spacing along the (110) plane, in contrast with the conventional spacing of 0.58 nm in previous reports (Fig. 1d).<sup>19, 20</sup> Moreover, the expanded interchain spacing is also evident from lattice fringes at the edges, which could facilitate enhanced  $Na^+$  insertion/extraction. We suppose that the expanded interchain spacing could be ascribed to the producing of gas from  $NH_4VO_3$  in the synthetic process, which results in the interchain spacing expansion to form hierarchical nanosheets. Scanning transmission electron microscopy (STEM) and corresponding elemental maps reveal the even distribution of V and S around the hierarchical nanosheets (Fig. 1e, f).

As presented in Fig. 2a, most reflections in XRD pattern are well indexed to standard reference of  $VS_4$ . Notably, the characteristic peak of (110) plane is observed to be shifted to  $8.8^\circ$  and the corresponding interchain spacing could be calculated to be 0.99 nm based on Bragg's law equation.<sup>16</sup> The calculated expanded interchain spacing is greater than previous reported spacing, agreeing well with TEM observation.<sup>19, 20</sup> This is also the first report of such a large interchain spacing in  $VS_4$ , which could allow for more  $Na^+$  to insert into the structures. The observed bands at  $139\text{ cm}^{-1}$ ,  $191\text{ cm}^{-1}$ ,  $281\text{ cm}^{-1}$ , and  $405\text{ cm}^{-1}$  from Raman spectrum are ascribed to characteristics of  $VS_4$  (Fig. 2b).<sup>26, 27</sup> The survey X-ray photoelectron spectra confirmed the presence of V and S elements in  $VS_4$  (Fig. S1). The curve-fitted peak components of V 2p at 524.2 eV and 516.8 eV, as well as 521.2 eV and 513.7 eV, are associated with  $V^{4+}$  and  $V^{3+}$ , respectively, which agrees well with previous reports.<sup>28-30</sup> Curve fitting of the S 2p spectrum yields three peaks: the binding energies at 163.5 eV and 162.3 eV are assigned to S  $2p_{1/2}$  and S  $2p_{3/2}$  of  $(S_2)^{2-}$ , respectively, while the binding energy at 161.1 eV is related to  $S^{2-}$ .<sup>21, 22, 27</sup> These characterization results confirmed the successful preparation of hierarchical  $VS_4$  nanosheets.

To gain deeper insight into the formation mechanism of hierarchical  $VS_4$  nanosheets, we have conducted experiments with different reaction times of 10 min, 30 min, and 1 h. Then we collected the TEM images and corresponding maps of these samples, as demonstrated in Fig. S2–4. Based on these observations, we propose the formation mechanism of hierarchical  $VS_4$  nanosheets, as demonstrated in Fig. S5. The evolution of crystal is revealed by XRD patterns with different reaction times (Fig. S6). The characteristic reflections of  $VS_4$  appeared when the reaction times reached up to 2 h.



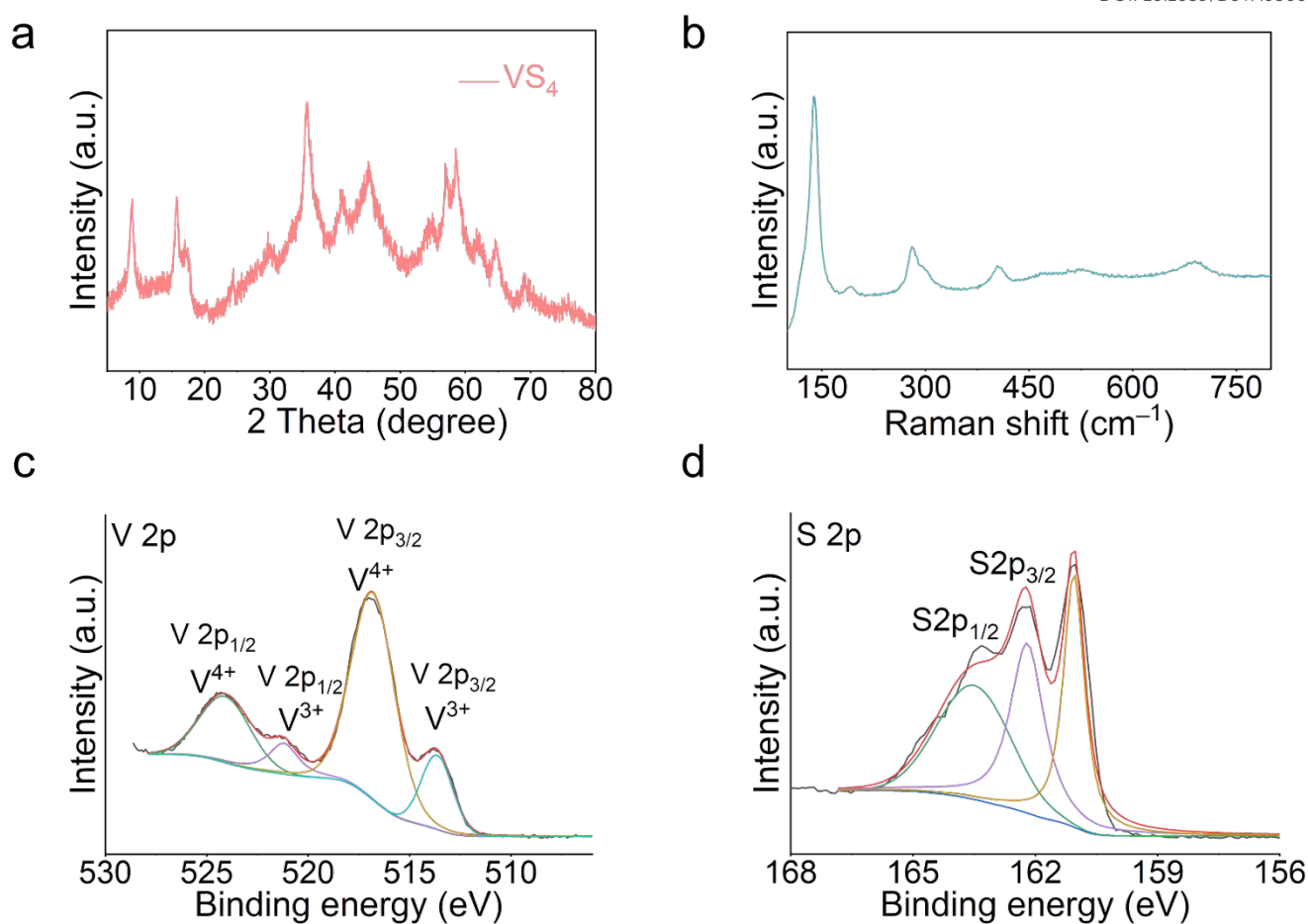


**Fig. 2 Materials characterizations:** (a) XRD pattern, (b) Raman spectrum, XPS spectra of (c) V 2p and (d) S 2p, respectively.

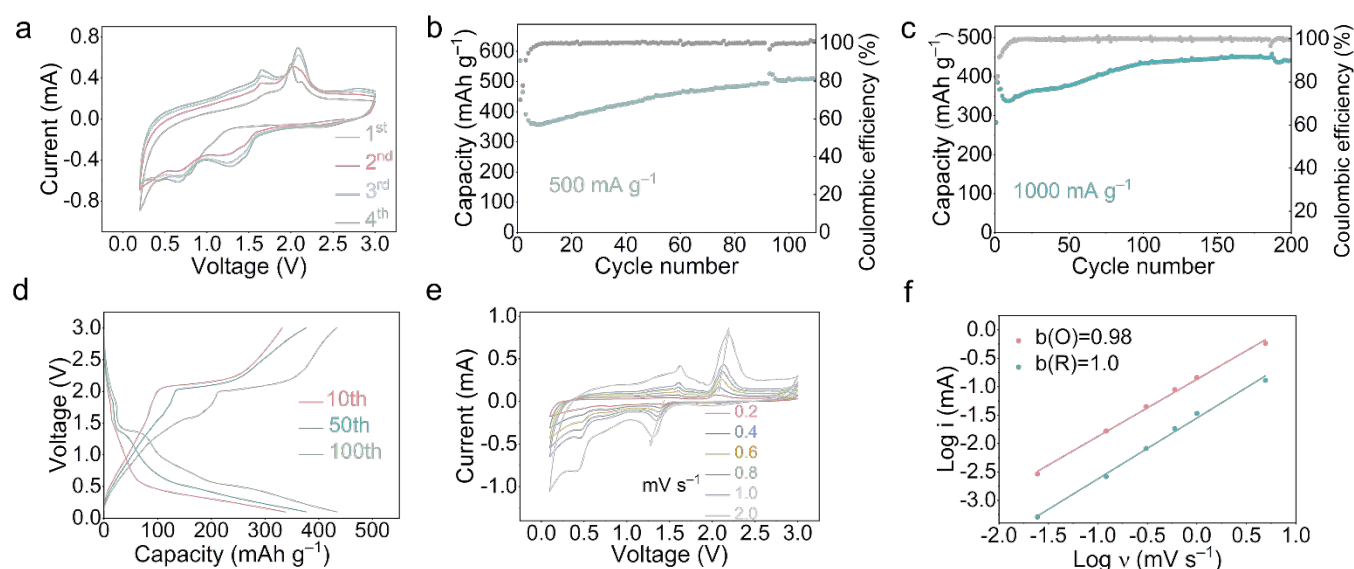


**Fig. 3 Electrochemical performances for hierarchical  $VS_4$  nanosheets:** (a) CV curves at  $0.5 \text{ mV s}^{-1}$ , cycling performance at current densities of (b)  $500 \text{ mA g}^{-1}$ , (c)  $1000 \text{ mA g}^{-1}$ , and (d) the corresponding charge–discharge profiles after different cycles at  $1000 \text{ mA g}^{-1}$ . (e) CV rates, (f) the corresponding calculated values of  $b$ .





We conducted a series of electrochemical tests to evaluate the effectiveness of the designed hierarchical VS<sub>4</sub> nanosheets in hosting Na<sup>+</sup>. CV curves were obtained at 0.5 mV s<sup>-1</sup>, in which the decreased voltage gap of redox peaks could be observed upon cycling (Fig. 3a). Moreover, the increasing intensity of redox peaks in the CV curves over successive cycles indicates reduced polarization and accelerated kinetics. Thereafter, the cycling performance was tested at 500 mA g<sup>-1</sup>, a stable capacity of 509 mAh g<sup>-1</sup> is achieved after 110 cycles (Fig. 3b). Even at a higher current density of 1000 mA g<sup>-1</sup> (Fig. 3c), the electrode can maintain a high capacity of 441 mAh g<sup>-1</sup> after 200 cycles, showing some advantages among reported VS<sub>4</sub>-based anodes in SIBs (Table S1).<sup>21, 31-41</sup> Furthermore, the plateaus observed in corresponding charge–discharge profiles at 1000 mA g<sup>-1</sup> agree well with the redox peaks in CV curves. Moreover, the charge–discharge profiles after 100<sup>th</sup> cycles demonstrate the smallest voltage gap between discharge and charge plateaus compared to the 10<sup>th</sup> and 50<sup>th</sup> cycles, further supporting the enhanced kinetics as observed in CV curves (Fig. 3d). In contrast, the electrode is short-circuited after 43 cycles with an inferior capacity of 75 mAh g<sup>-1</sup> when it was used in electrolytes based on NaPF<sub>6</sub>, reflecting the advantages of NaOTF electrolytes (Fig. S7). CV rates were performed to investigate the capacity contribution dominated from diffusion-controlled process or capacitance effect, based on the following equation:

$$i = av^b \quad (1)$$

$i$  is the current,  $a$  and  $b$  are constant characters,  $v$  is the sweep rate (Fig. 3e). The calculated  $b$  values represent the electrochemical process is dominated by capacitance effect or diffusion-controlled process, when the values of  $b$  are close to 1 or 0.5, respectively. The calculated values of  $b$  are 1.0 and 0.98 at anodic and cathodic peaks, respectively (Fig. 3f). These results indicate that the electrochemical process was dominated by capacitance effect. The specific contribution from capacitance can be evaluated using the following equation:

$$i = k_1v + k_2v^{1/2} \quad (2)$$

in which  $i$  is the current,  $v$  is the sweep rate,  $k_1$ , and  $k_2$  are constants. The calculated results indicate that capacitive contribution increases with increasing sweep rates. In specific, the capacitive contribution approaches to 90.2 % at a sweep rate of 1 mV s<sup>-1</sup> (Fig. S8). To further demonstrate the benefits of the designed hierarchical VS<sub>4</sub> nanosheets, electrochemical impedance spectroscopy (EIS) shows a significantly lower impedance after 20 cycles than that after 3 cycles, indicating improved kinetics with ongoing cycling (Fig. S9).

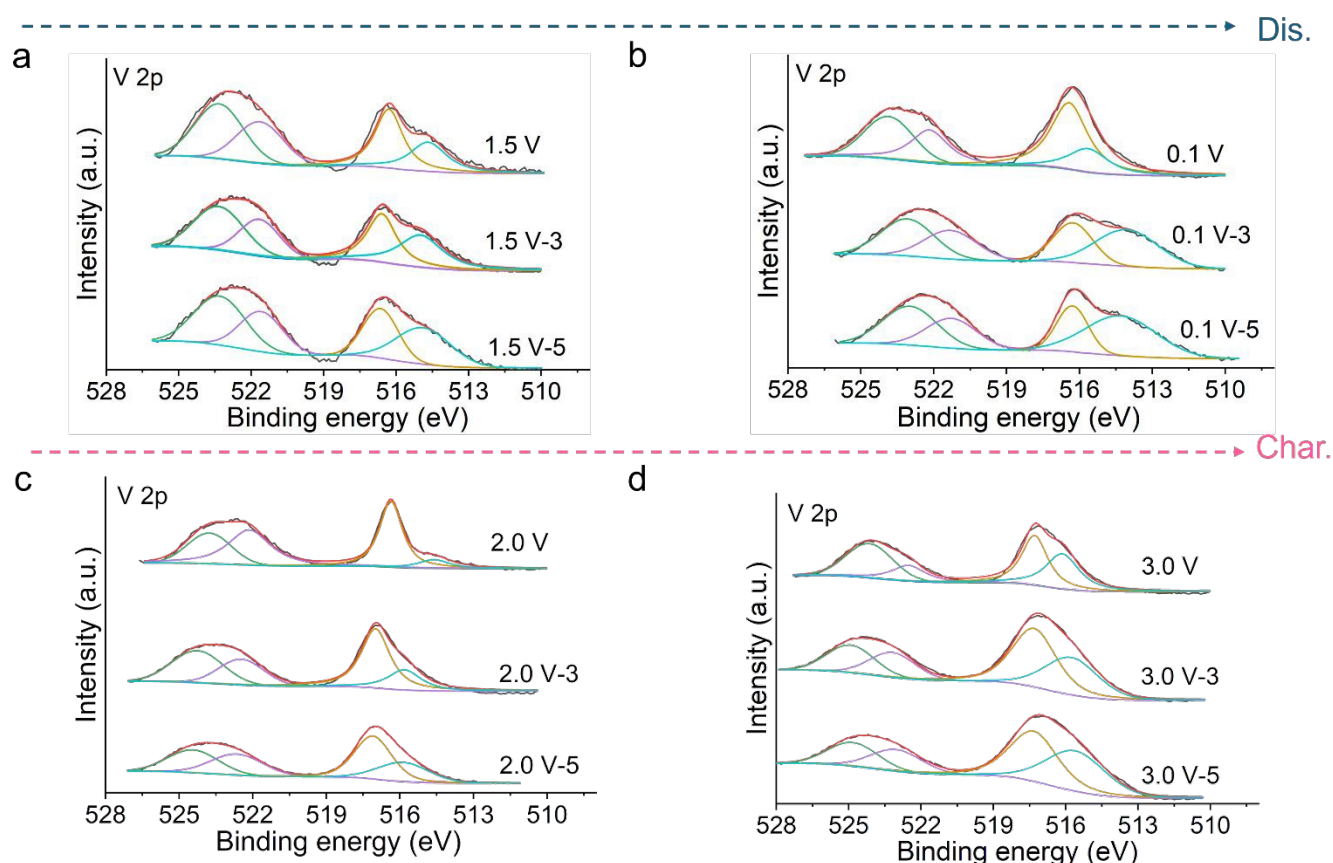


**Fig. 4** Ex-situ XPS spectra of V 2p from samples at different potential states of (a) 1.5 V, (b) 0.1 V, (c) 2.0 V, and (d) 3.0 V.



XPS depth profiling and synchrotron XAS spectra are used to understand the storage mechanism and interfacial chemistry between hierarchical  $\text{VS}_4$  nanosheets and electrolytes (Fig. 4–7). Ex-situ XPS spectra were collected from samples at different potential states of 1.5 V, 0.01 V, 2.0 V, and 3.0 V. The data labelled 1.5 V, 1.5 V–3, and 1.5 V–5 represent these samples are treated with etching times of 0 min, 3 mins, and 5 mins, respectively (The notation applies to other potential states as well). Upon discharge to 1.5 V, the intensity peaks for  $\text{V}^{4+}$  increases while  $\text{V}^{3+}$  decreases in contrast with pristine sample. This should be attributed to insertion of  $\text{Na}^+$  and transfer of electrons within  $\text{VS}_4$  and formation of  $\text{Na}_3\text{VS}_4$ .<sup>21</sup> No significant differences in V 2p are observed among the 1.5 V, 1.5 V–3, 1.5 V–5 samples. Upon further discharge to 0.1 V, the intensity ratio for  $\text{V}^{4+}/\text{V}^{3+}$  increases at the electrode surface, while it decreases in both 0.1 V–3 and 0.1 V–5. This suggests the co-existence of insertion/conversion reactions during the discharge process, with the high  $\text{V}^{4+}/\text{V}^{3+}$  intensity ratio at 0.1 V likely attributed to the surface oxidation in the process of measurements.

During the subsequent charge process, the binding energies of V 2p at 2.0 V are higher than those at 1.5 V and 0.1 V, which comes from the presence of  $\text{V}^{5+}$ .<sup>28</sup> More importantly, the binding energies of V 2p at 2.0 V–3 and 2.0 V–5 are similar but higher than those at 2.0 V, suggesting that the degree of insertion reaction is greater within the bulk of the material than at the surface. Upon full charging to 3.0 V, the V 2p binding energies shift further to higher values, demonstrating partial reversibility of the insertion reactions. These results suggest that  $\text{Na}_3\text{VS}_4$  remains partially unconverted, with only partial reversibility of the conversion reactions. Therefore, the final product at full charge state is likely a composite of  $\text{Na}_3\text{VS}_4$  ( $\text{V}^{5+}$ ) and  $\text{VS}_4$  ( $\text{V}^{4+}$ ), which is different from previous reports that use NaOTf-based ether electrolyte.<sup>21, 30</sup>

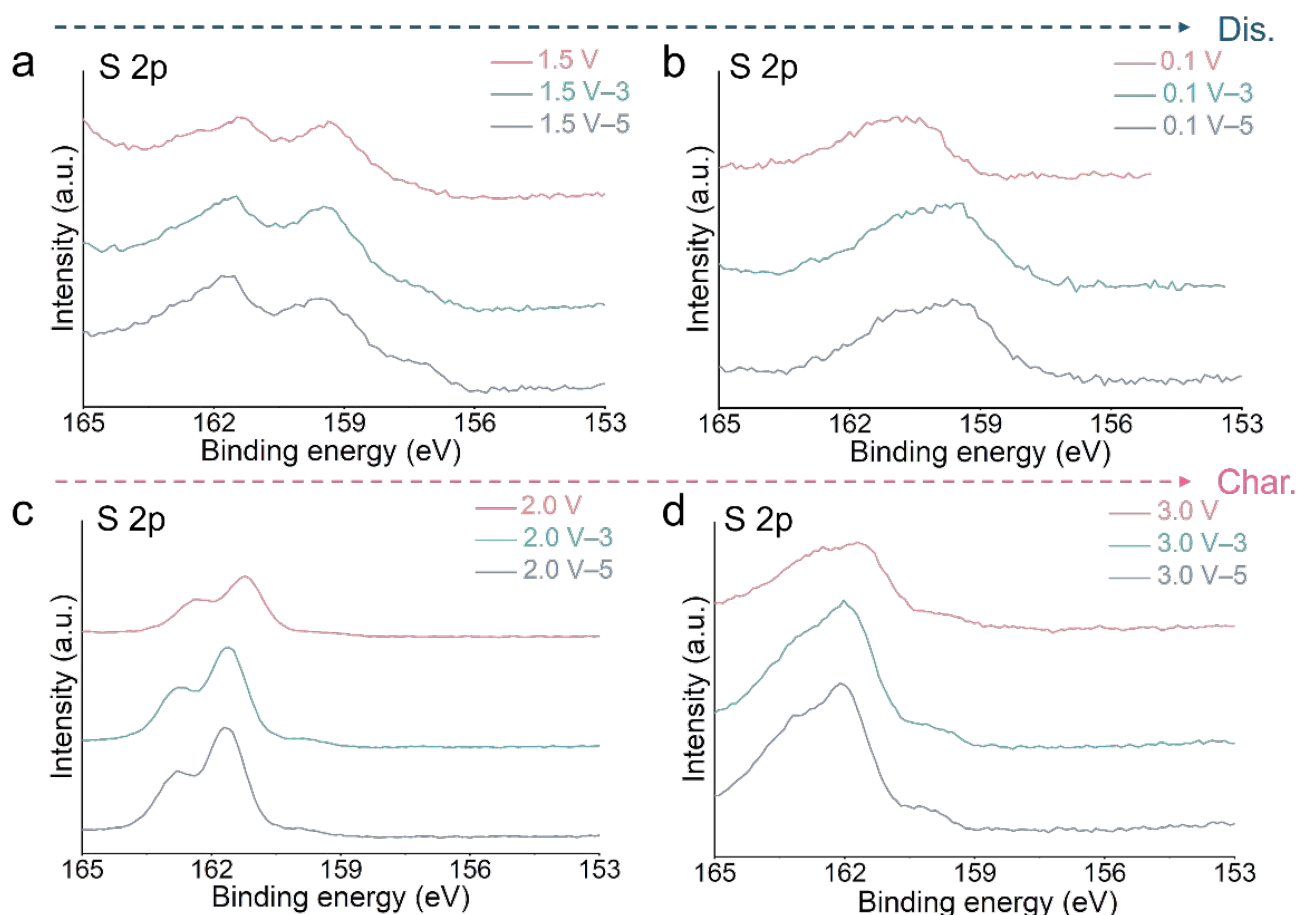


**Fig. 5** Ex-situ XPS spectra of S 2p collected at different voltages of (a) 1.5 V, (b) 0.1 V, (c) 2.0 V, and (d) 3.0 V, respectively.



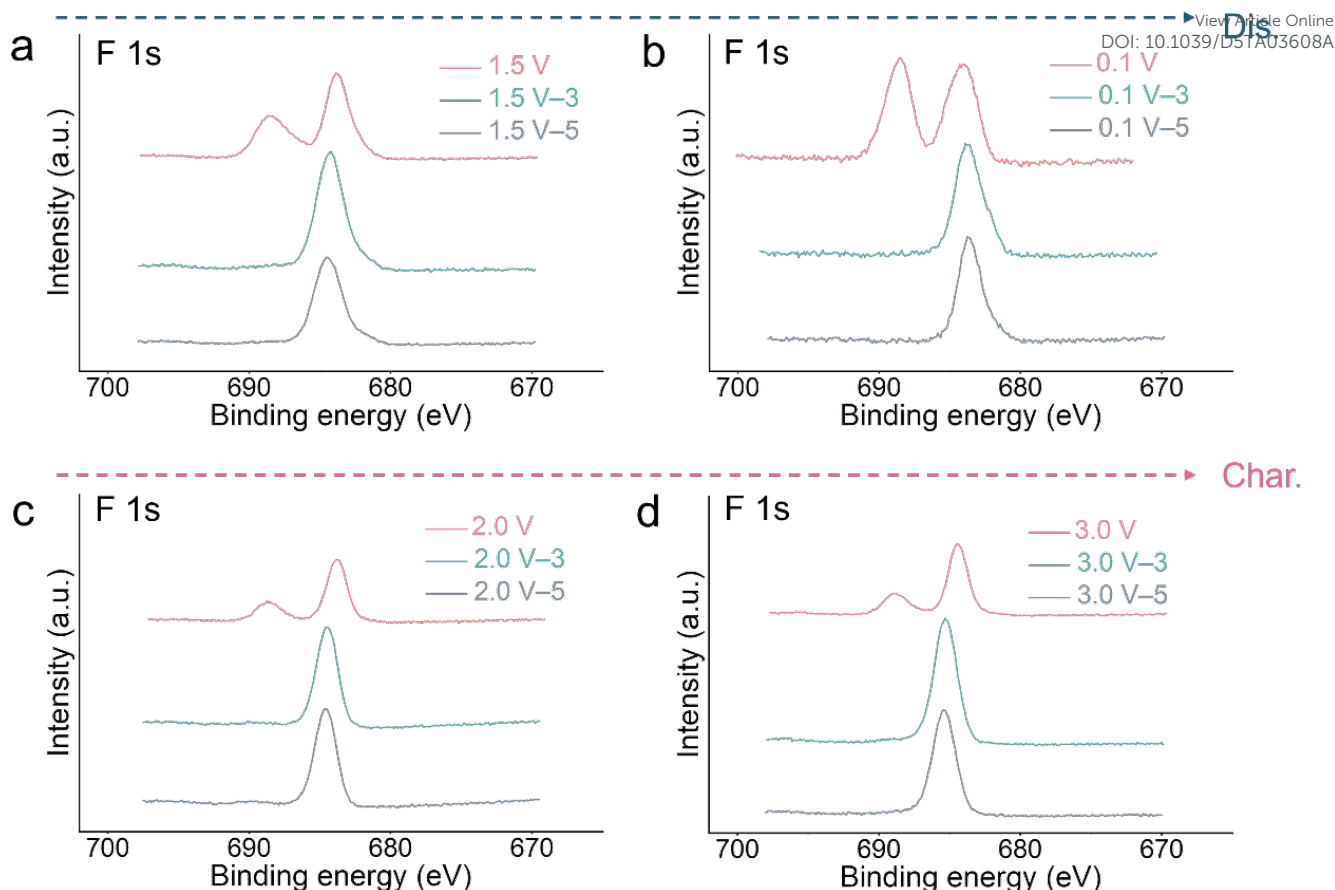


**Fig. 6** Ex-situ XPS spectra of F 1s collected at different voltages of (a) 1.5 V, (b) 0.1 V, (c) 2.0 V, and (d) 3.0 V, respectively.

We have also investigated the composition of solid electrolyte interphase (SEI) formed on the surface of anode after two cycles (Fig. 6, S10). In detail, the deconvoluted F 1s spectra show binding energies at 688.5 eV and 683.7 eV, corresponding to Na-F and C-F bonds, respectively.<sup>11, 42</sup> The disappearance of C-F peak after the etching treatment, suggesting the C-F bonds originates from electrolytes. Moreover, the binding energy for Na-F binding can be observed at different etching times, indicating the formation of a stable NaF-rich SEI layer. The corresponding Na 1s XPS spectra collected from different potential states also supported the presence of SEI formed on hierarchical VS<sub>4</sub> nanosheets, accounting for the superior electrochemical sodium storage performance.

XAS spectra at different potential states were collected to gain deeper understanding of the energy storage mechanism (Fig. 7a, b). The K-edge of V shifts to higher photon energy in contrast to the sample at open circuit voltage (OCV) throughout the discharge/charge process, which was attributed to the insertion of Na<sup>+</sup> and the formation of Na<sub>3</sub>VS<sub>4</sub>. Notably, at the discharge cut-off voltage of 0.1 V, the V K-edge approaches to that of OCV, suggesting a hybrid mechanism involving both conversion and insertion. In the converse charge potential states of 0.8 V and 3.0 V, the V K-edges further shift to higher energy regions relative to 0.1 V and OCV. These observations confirm that the insertion reactions dominate the entire electrochemical process at the bulk level, aligning well with ex-situ XPS results.





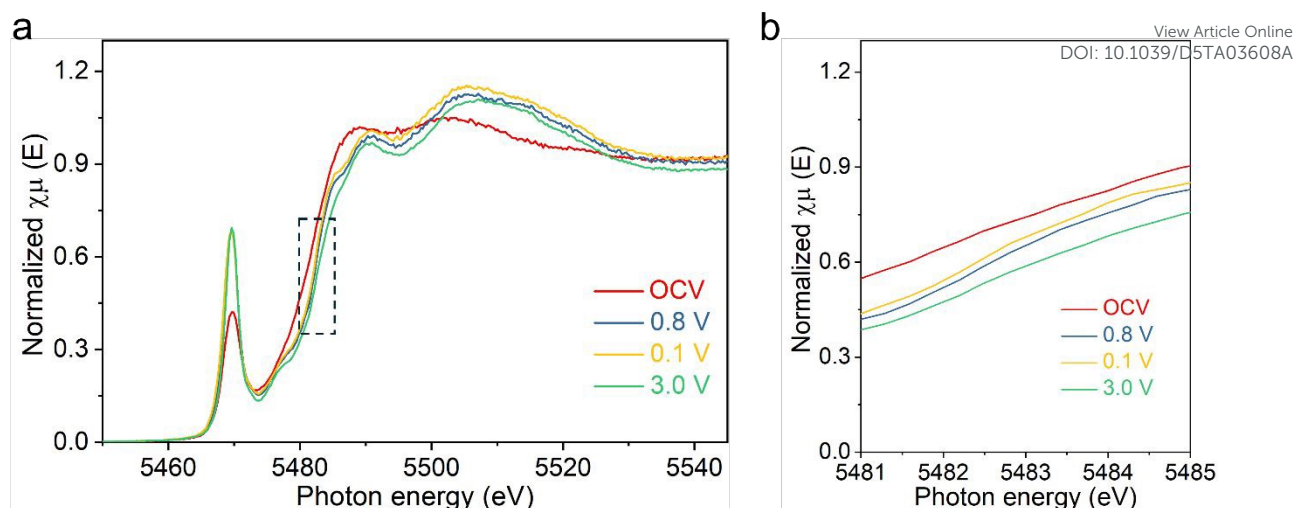


**Fig. 7** (a) XAS spectra collected at different potential states, and (b) corresponding magnified part of K-edge.

To highlight the advantages of hierarchical VS<sub>4</sub> nanosheets, we compared the stress and corresponding displacements between solid spheres and hierarchical nanosheets structures of VS<sub>4</sub> under free boundary conditions (Fig. 8). The average stress in solid spheres and hierarchical nanosheets are simulated to be similar (Fig. 8a, c). However, the average displacement in solid spheres (22.8 nm) is higher than that in hierarchical nanosheets (19.8 nm). (Fig. 8b, d) Notably, displacement in the hierarchical nanosheets is mainly located at the outer edges, providing sufficient space to allow for volume change. In contrast, there is no space for solid spheres to undergo expansion, making them prone to cracking during cycling. So, these results demonstrate that the rational design of hierarchical nanosheets effectively mitigates mechanical stress and enhances electrochemical performance.

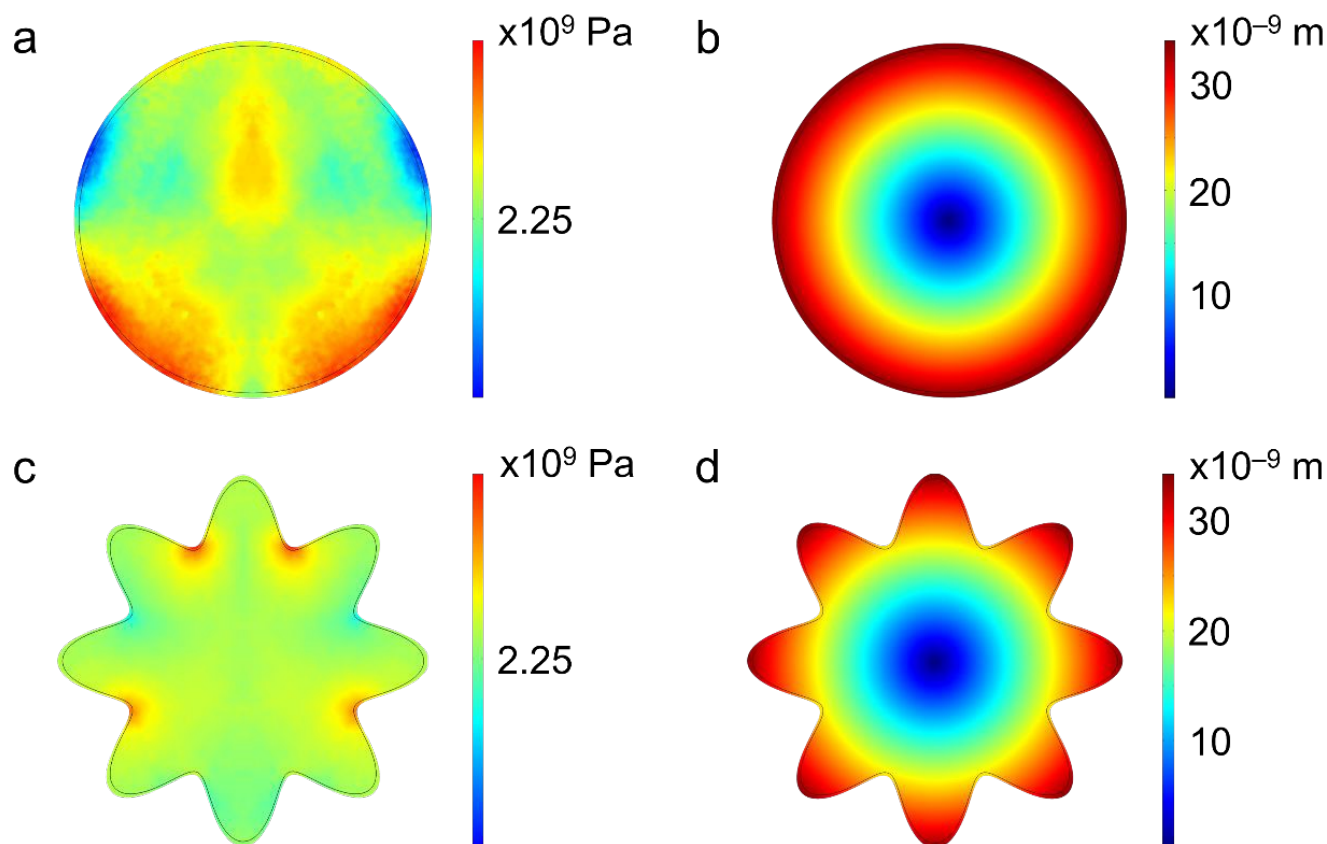


**Fig. 8 FES simulations:** (a, c) Stress distributions in solid spheres and hierarchical VS<sub>4</sub> nanosheets, respectively. (b, d) Total displacements in solid spheres and hierarchical VS<sub>4</sub> nanosheets, respectively.



Computer tomography (CT) of pouch cells before cycling and after 20 cycles is used to investigate the volume changes of hierarchical VS<sub>4</sub> nanosheets (Fig. S11). The cross-section CT slices show no significant change in the anode thickness after 20 cycles, which is consistent with the FES simulations. Moreover, TEM image and corresponding elemental maps of the electrode after 20 cycles reveal that the hierarchical nanosheets morphology can be well maintained, supporting the structural stability of hierarchical VS<sub>4</sub> nanosheets (Fig. S12).

## 4. Conclusions

In this work, we have developed hierarchical VS<sub>4</sub> nanosheets with expanded interchain distance for the first time via a one-step solvothermal process without the use of additives. The expanded interchain distance can accommodate more insertion/extraction of Na<sup>+</sup>, while the porous hierarchical nanosheets can alleviate the volume variation and reduce the diffusion pathway of Na<sup>+</sup> in the electrochemical process, as supported by data from FES simulations. Furthermore, we uncovered an insertion behavior dominated sodium storage mechanism via ex-situ XPS and XAS spectra. As such, the optimized anode demonstrates a high capacity of 441 mAh g<sup>-1</sup> after 200 cycles at 1 A g<sup>-1</sup>, highlighting the advantages of rationally designed hierarchical nanosheets structures. This work emphasizes the importance of engineering in both morphology and internal structure (e.g., interchain spacing) to achieve superior electrochemical performance. Moreover, this work also offers new insights into the working principles of VS<sub>4</sub> in SIBs. Future research will focus on further elucidating electrode storage mechanisms to advance the understanding and development of high-performance battery systems.

## Author contributions

J. W., P. C., and W. L. contributed equally to this work. J. W. and Z. W. S. conceived the original concept and initiated the project. J. W. wrote the manuscript. M. W., H. W. and Z. W. S. revised it. P. C. synthesized the materials and performed the electrochemical performance test. Z. A. (TEM), S. S. (XRD), W. L. (XAS), W. B. (XAS), L. Z. carried out the simulations.

## Conflicts of interest

There are no conflicts to declare.

## Data availability

A data availability statement (DAS) is required to be submitted alongside all articles. Please read our [full guidance on data availability statements](#) for more details and examples of suitable statements you can use.

## Acknowledgements

Z. W. Seh acknowledges support by the Singapore National Research Foundation (NRF Investigatorship NRF-NRFI09-0002) and the Agency for Science, Technology and Research (MTC Programmatic Fund M23L9b0052).

## References

1. Y. Liang and Y. Yao, *Nat. Rev. Mater.*, 2022, **8**, 109-122.
2. A. Y. S. Eng, C. B. Soni, Y. Lum, E. Khoo, Z. Yao, S. Vineeth, V. Kumar, J. Lu, C. S. Johnson and C. Wolverton, *Sci. Adv.*, 2022, **8**, eabm2422.
3. J. Wang, G. Yang, T. Ghosh, Y. Bai, C. Y. J. Lim, L. Zhang, D. H. L. Seng, W. P. Goh, Z. Xing, Z. Liu and Z. W. Seh, *Nano Energy*, 2024, **119**.
4. J. Wang, T. Ghosh, Z. Ju, M.-F. Ng, G. Wu, G. Yang, X. Zhang, L. Zhang, A. D. Handoko and S. Kumar, *Matter*, 2024, **7**, 1833-1847.
5. J. Wang and Z. W. Seh, *Acc. Mater. Res.*, 2024, **5**, 1329-1339.
6. J. Wang, N. Luo, J. Wu, S. Huang, L. Yu and M. Wei, *J. Mater. Chem. A*, 2019, **7**, 3691-3696.
7. J. Wang, L. Han, X. Li, L. Zeng and M. Wei, *J. Colloid Interf. Sci.*, 2019, **548**, 20-24.
8. Y. Gao, Z. Wang, H. Tu, J. Xue, S. Weng, S. Lu, L. Liu, G. Sun, K. Peng, X. Zhang, D. Li, Y. Liu, J. Xu, H. Li and X. Wu, *Adv. Funct. Mater.*, 2024, **35**.
9. C. Liu, K. Chen, F. Li, A. Zhao, P. Liu, Z. Chen, Y. Fang and Y. Cao, *J Am Chem Soc*, 2025, **147**, 14635-14646.
10. H. Chen, K. Chen, J. Yang, B. Liu, L. Luo, H. Li, L. Chen, A. Zhao, X. Liang, J. Feng, Y. Fang and Y. Cao, *J Am Chem Soc*, 2024, **146**, 15751-15760.
11. Z. W. Seh, J. Sun, Y. Sun and Y. Cui, *ACS Cent Sci*, 2015, **1**, 449-455.



12. X. Lu, H. Zhao, Y. Qin, E. Matios, J. Luo, R. Chen, H. Nan, B. Wen, Y. Zhang, Y. Li, Q. He, X. Deng, J. Lin, K. Zhang, H. Wang, K. Xi, Y. Su, X. Hu, *ACS Nano*, 2023, **17**, 10665-10676. DOI: 10.1039/D5TA03608A
13. C. Wang, A. C. Thenuwara, J. Luo, P. P. Shetty, M. T. McDowell, H. Zhu, S. Posada-Perez, H. Xiong, G. Hautier and W. Li, *Nat. Commun.*, 2022, **13**, 4934.
14. A. Rudola, R. Sayers, C. J. Wright and J. Barker, *Nat. Energy*, 2023, **8**, 215-218.
15. C. Vaalma, D. Buchholz, M. Weil and S. Passerini, *Nat. Rev. Mater.*, 2018, **3**, 1-11.
16. F. Zhang, B. He, Y. Xin, T. Zhu, Y. Zhang, S. Wang, W. Li, Y. Yang and H. Tian, *Chem. Rev.*, 2024, **124**, 4778-4821.
17. Y. Zhao, Y. Kang, J. Wozny, J. Lu, H. Du, C. Li, T. Li, F. Kang, N. Tavajohi and B. Li, *Nat. Rev. Mater.*, 2023, **8**, 623-634.
18. J. Wang, L. Yu, Z. Zhou, L. Zeng and M. Wei, *J. Colloid Interf. Sci.*, 2019, **557**, 722-728.
19. J. Wang, J. Huang, S. Huang, H. Notohara, K. Urita, I. Moriguchi and M. Wei, *ACS Sustain. Chem. & Eng.*, 2020, **8**, 9519-9525.
20. J. Wang, J. Okabe, K. Urita, I. Moriguchi and M. Wei, *J. Electroanal. Chem.*, 2020, **874**, 114523.
21. S. Wang, F. Gong, S. Yang, J. Liao, M. Wu, Z. Xu, C. Chen, X. Yang, F. Zhao, B. Wang, Y. Wang and X. Sun, *Adv. Funct. Mater.*, 2018, **28**, 1801806.
22. L. q. Yu, S. X. Zhao, Q. I. Wu, J. W. Zhao and G. d. Wei, *Adv. Funct. Mater.*, 2020, **30**, 2000427.
23. Z. Wang, X. Li, W. Guo and Y. Fu, *Adv. Funct. Mater.*, 2021, **31**, 2009875.
24. D. Zhang, Y. Shao, J. Wang, Z. Li, Q. Wang, H. Sun, Q. Sun and B. Wang, *Small Struct.*, 2023, **5**, 2300217.
25. M. Tang, X. Yin, Y. Cao, H. Ma, X. Zhang and D. Jia, *Small*, 2024, **20**, e2406547.
26. D. Zhang, Y. Shao, J. Wang, Z. Li, Q. Wang, H. Sun, Q. Sun and B. Wang, *Small*, 2024, **20**, e2309901.
27. D. Yang, S. Zhang, P. Yu, S. Cheng, Z. Yuan, Y. Jiang, W. Sun, H. Pan, Y. Feng, X. Rui and Y. Yu, *Small*, 2022, **18**, e2107058.
28. P. Yu, S. Xu, K. Yao, H. Yao, W. Yang, X. Lin, H. Yu, W. Liu, Y. Qin and X. Rui, *J. Power Sources*, 2021, **501**, 230021.
29. W. Li, J. Huang, R. Li, L. Cao, X. Li, L. Feng and S. Chen, *Chem. Eng. J.*, 2020, **384**, 123385.
30. Z. Qin, Y. Hu, C. Lv, S. Yao and G. Chen, *Chem. Eng. J.*, 2022, **433**, 133765.
31. L. Song, Y. Tang, R. Mao, J. Sun, C. Yu, Y. Liu and Y. Zhao, *ACS Appl. Nano Mater.*, 2024, **7**, 9002-9011.
32. W. Li, J. Huang, R. Li, L. Cao, X. Li, S. Chen and L. Feng, *ChemSusChem*, 2019, **12**, 5183-5191.
33. X. Li, H. Liang, B. Qin, M. Wang, Y. Zhang and H. Fan, *J. Colloid Interf. Sci.*, 2022, **625**, 41-49.
34. F. Yang, W. Zhong, H. Wang, M. Ren, W. Liu, M. Li and L. Su, *J. Alloys and Compd.*, 2020, **834**, 155204.
35. R. Sun, Q. Wei, Q. Li, W. Luo, Q. An, J. Sheng, D. Wang, W. Chen and L. Mai, *ACS Appl. Mater. Interf.*, 2015, **7**, 20902-20908.
36. W. Li, J. Huang, L. Cao, L. Feng and C. Yao, *Electrochim. Acta*, 2018, **274**, 334-342.
37. W. Li, J. Huang, L. Feng, L. Cao and S. He, *Nanoscale*, 2018, **10**, 21671-21680.
38. X. Zhang, Q. He, X. Xu, T. Xiong, Z. Xiao, J. Meng, X. Wang, L. Wu, J. Chen and L. Mai, *Adv. Energy Mater.*, 2020, **10**.
39. Y. Yi, X. Du, Z. Zhao, Y. Liu, H. Guan, X. Liu, X. Pei, S. Zhang and D. Li, *ACS Nano*, 2022, **16**, 7772-7782.
40. K. H. Kim, J. Choi and S. H. Hong, *Chem. Commun. (Camb)*, 2019, **55**, 3207-3210.
41. Y. Zeng, J. Yang, H. Yang, Y. Yang and J. Zhao, *ACS Energy Lett.*, 2024, **9**, 1184-1191.
42. J. Song, B. Xiao, Y. Lin, K. Xu and X. Li, *Adv. Energy Mater.*, 2018, **8**.



The data supporting this article has been included as part of the ESI

[View Article Online](#)  
DOI: 10.1039/D5TA03608A

Open Access Article. Published on 31 2025. Downloaded on 08/08/25 13:49:45.  
This article is licensed under a Creative Commons Attribution-NonCommercial 3.0 Unported Licence.

